Colossal terahertz magnetoresistance at room temperature in epitaxial $La_{0.7}Sr_{0.3}MnO_3$ nanocomposites and single-phase thin films

J. Lloyd-Hughes,[*,†] C. D. W. Mosley,[†] S. P. P. Jones,[‡] M. R. Lees,[†] A. Chen,[¶] Q.X. Jia,[§] E.-M. Choi,[‖] and J. L. MacManus-Driscoll[‖]

University of Warwick, Department of Physics, Gibbet Hill Road, Coventry, CV4 7AL, United Kingdom., University of Oxford, Department of Physics, Clarendon Laboratory, Parks Road, Oxford, OX1 3PU, United Kingdom., Center for Integrated Nanotechnologies, Los Alamos National Laboratory, Los Alamos, NM 87545, USA., Materials Design and Innovation, School of Engineering and Applied Sciences, University at Buffalo, 311 Bell Hall, Buffalo, NY 14260-5030, USA., and University of Cambridge, Department of Materials Science, 27 Charles Babbage Road, Cambridge, CB3 0FS, United Kingdom.

E-mail: j.lloyd-hughes@warwick.ac.uk

Abstract

Colossal magnetoresistance (CMR) is demonstrated at terahertz (THz) frequencies by using terahertz time-domain magnetospectroscopy to examine vertically-aligned

---

*To whom correspondence should be addressed
†University of Warwick
‡University of Oxford
¶Los Alamos National Laboratory
§University at Buffalo
‖University of Cambridge

nanocomposites (VANs) and planar thin films of $La_{0.7}Sr_{0.3}MnO_3$. At the Curie temperature (room temperature) the THz conductivity of the VAN was dramatically enhanced by over 2 orders of magnitude under the application of a magnetic field, with a non-Drude THz conductivity that increased with frequency. The dc CMR of the VAN is controlled by extrinsic magnetotransport mechanisms such as spin-polarized tunneling between nano-grains. In contrast, we find that THz CMR is dominated by intrinsic, intragrain transport: the mean free path was smaller than the nanocolumn size, and the planar thin-film exhibited similar THz CMR to the VAN. Surprisingly, the observed colossal THz magnetoresistance suggests that the magnetoresistance can be large for ac motion on nanometre length scales, even when the magnetoresistance is negligible on the macroscopic length scales probed by dc transport. This suggests that colossal magnetoresistance at THz frequencies may find use in nanoelectronics and in THz optical components controlled by magnetic fields. The VAN can be scaled in thickness while retaining a high structural quality, and offers a larger THz CMR at room temperature than the planar film.

Keywords

Perovskite oxides; Oxide nanocomposites; Colossal magnetoresistance; Terahertz radiation; Conductivity

Introduction

The colossal magnetoresistance (CMR) of manganite compounds such as $La_{0.7}Sr_{0.3}MnO_3$ can arise from intrinsic or extrinsic mechanisms.[1] At temperatures below the Curie temperature T_C the half-metallic ferromagnet $La_{0.7}Sr_{0.3}MnO_3$ exhibits a finite density of states in the majority spin band at the chemical potential, while the minority spin channel has a gap.[2] The *intrinsic* magnetoresistance (MR) of pure single crystals of $La_{0.7}Sr_{0.3}MnO_3$ is linked to the double-exchange picture of charge transport, where core Mn 3d t_{2g} spins mediate

charge transport. Carriers can travel within the majority band, derived from Mn 3d e_g and O 2p orbitals,[2] when neighbouring Mn core spins are aligned. In high quality single crystals, the intrinsic MR is peaked close to T_C, and large magnetic fields >1 T are often needed to produce substantial changes in resistance.[1] Here and elsewhere the MR is defined as $\Delta\rho/\rho_0 = (\rho_B - \rho_0)/\rho_0$, where ρ_B and ρ_0 are the resistivity with and without a magnetic field B.

Large *extrinsic* magnetoresistance is found in polycrystalline and thin-film manganites: it often requires lower magnetic fields, peaks at temperatures below T_C, and results from spin-polarized tunneling between different grains.[1,3,4] Adding a second inert material (e.g. a non-magnetic insulator) creates more grain boundaries, boosting structural, chemical and spin disorder at interfaces, all of which influence the magnetoresistance.[4,5] Pulsed laser deposition (PLD) is an ideal way to create such systems as the materials can spontaneously form vertically-aligned nanocomposites (VANs) of the ferromagnetic and inert phases, giving considerable control and tunability over the nature of the interfaces.[6–8] For instance the distance between ferromagnetic grains, and the width of the spin-disordered interfacial region, can be altered by varying the deposition frequency, yielding an enhanced extrinsic MR for smaller grain sizes.[9] Strained, single-phase films can be grown with larger thicknesses than their epitaxial planar counterparts, owing to the structural support given by the scaffold of the inert phase.

The magneto-optical response at THz frequencies is a powerful probe of material properties, allowing carrier masses[10,11] and spin-orbit coupling strengths[12] to be uncovered for conducting systems. Interesting physical phenomena such as the quantum Hall effect[13] and the giant magnetoresistance of ferromagnetic metals[14] have been found to persist up to THz frequencies. In metal heterostructures exhibiting giant magnetoresistance a study of the THz magnetoconductivity found similar THz and dc magnetoresistances, with changes of around 20 % in the THz conductivity induced by $B = 100\,\text{mT}$.[14] Turning to oxide systems, colossal magnetoresistance has not been studied at THz frequencies. In the CMR com-

pounds, changes in the mid-infrared conductivity under a magnetic field were assigned to bipolarons breaking into polarons.[15,16] Without a magnetic field, free-carrier absorption in $La_{0.7}Sr_{0.3}MnO_3$ in the far-infrared (THz) was found to follow the Drude lineshape, indicating delocalized intraband transport.[17–20]

Here we report for the first time that colossal magnetoresistance exists at THz frequencies, both for a VAN consisting of $La_{0.7}Sr_{0.3}MnO_3$ nanocolumns embedded within a ZnO scaffold, and for pure $La_{0.7}Sr_{0.3}MnO_3$ films. The THz CMR $\Delta\rho/\rho_0$ (for ac resistivity ρ) was found to grow towards the Curie temperature, reaching -99.9 % for the VAN at 300 K, corresponding to a change by more than 2 orders of magnitude in the THz conductivity. In contrast, the dc CMR for VANs peaks below T_C.[9] The length scale for charge transport was estimated from the measured carrier densities and scattering times, and found to be smaller than the grain size at all temperatures below the Curie temperature. Thus the conductivity at THz frequencies and the colossal THz MR appear to be linked to transport within the $La_{0.7}Sr_{0.3}MnO_3$ grains, rather than an extrinsic effect (e.g. spin-polarized tunneling) associated with the interfaces.

Results and discussion

Epitaxial $La_{0.7}Sr_{0.3}MnO_3$:ZnO VAN thin films were grown on (001)-oriented $LaAlO_3$ substrates by pulsed laser deposition.[3,9] This substrate was chosen for its good transparency in the THz region,[21] and the proximity of its lattice constant to that of bulk $La_{0.7}Sr_{0.3}MnO_3$. VANs of separate phases of $La_{0.7}Sr_{0.3}MnO_3$ and ZnO were formed as shown schemetically in Fig. 1(a), with grain widths of around 10 nm, as established previously using transmission electron microscopy.[3,9] A reference sample of $La_{0.7}Sr_{0.3}MnO_3$ without ZnO was grown under similar conditions.

High resolution X-ray diffraction was used to examine the crystal structure at room temperature. Fig. 1(b) shows $2\theta - \omega$ scans, where the VAN film exhibits a single (002)
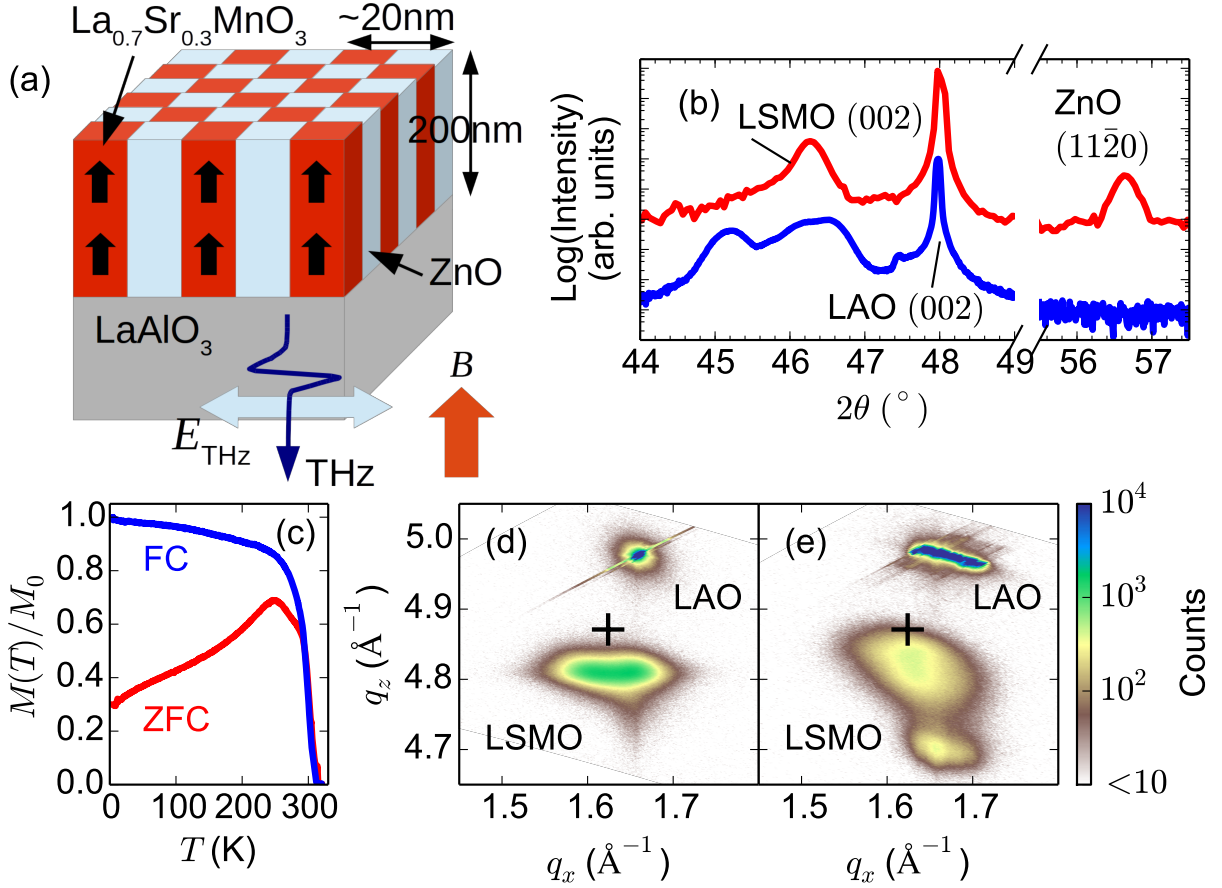
Figure 1: (a) Schematic of VAN film and THz spectroscopy experiment. The directions of the applied d.c. magnetic field B, THz pulse propagation vector and THz electric field E_{THz} are shown. Thick black arrows show the Mn magnetic moments. (b) X-ray diffraction scans around the (002) peaks of $LaAlO_3$ and $La_{0.7}Sr_{0.3}MnO_3$ for the VAN film (top) and the pure film (bottom), and around $(11\bar{2}0)$ for ZnO. (c) Normalized magnetization $M(T)/M_0$ under $B = 10\,\mathrm{mT}$ for field-cooled (FC) and zero-field-cooled (ZFC) cases. (d) Reciprocal space map around the (103) peaks for $LaAlO_3$ and $La_{0.7}Sr_{0.3}MnO_3$ for the VAN film. Cross: (103) position for bulk $La_{0.7}Sr_{0.3}MnO_3$. (e) Similar to (d) but for the pure $La_{0.7}Sr_{0.3}MnO_3$ film.

peak around $2\theta = 46.3°$, below the LaAlO$_3$ (002) peak at 48.0°. The single, sharp peak arises owing to vertical epitaxy with the ZnO phase, rather than strain control from the LaAlO$_3$ substrate. In contrast, the pure LSMO film exhibits multiple peaks as a result of strain relaxation away from the substrate. In-plane lattice constants were found from the (103) reciprocal space maps reported in Figs. 1(d) and (e). The VAN film had $a = 3.862$ Å, $c = 3.924$ Å, while the pure film consisted of a component lattice-matched to the LaAlO$_3$ substrate (which has a pseudocubic lattice constant 3.789 Å) with $a = 3.783$ Å, $c = 4.017$ Å, and a relaxed component with $a = 3.845$ Å, $c = 3.913$ Å. The in-plane lattice constant a for both the VAN and the relaxed component of the pure film are similar to that of bulk LSMO (3.870 Å).[9]

The interplanar spacing for ZnO for the (11$\bar{2}$0) peak is $d_{(11\bar{2}0)} = 3.249$ Å, giving $6d_{(11\bar{2}0)} = 19.63$ Å. This is close to $5d_{(001)} = 19.49$ Å for LSMO, and thus for every 5 LSMO unit cells vertically there are 6 ZnO (11$\bar{2}$0) planes, as for LSMO:ZnO VAN films on SrTiO$_3$ substrates.[9]

In Fig. 1(c) the normalized magnetization $M(T)/M_0$ is reported for field-cooled (FC) and zero-field-cooled cases. The reduction in the Curie temperature to $T_C = 303$ K for the VAN film in comparison to $T_C = 353$ K for the pure LSMO film (data not shown) may arise from the lower volume fraction of LSMO grains in the VAN film,[9] which lowers the mean magnetic field on each core spin.

The complex optical conductivity $\sigma(\omega)$ was calculated from the complex transmission, treating the VAN film as a uniform effective medium.[22] Previous work has shown that the ac THz conductivity of pure LSMO films exhibits free-carrier-like behaviour,[17–20] following the Drude-Lorentz model of free-carrier absorption.[22] In this model $\sigma(\omega) = \sigma_0/(1 + i\omega\tau)$ for dc conductivity $\sigma_0 = Ne^2\tau/m^*$, where the carrier density, scattering time and mass are N, τ and m^* respectively. Hence the real conductivity $\sigma_1(\omega)$ peaks at zero frequency, with amplitude σ_0. In Fig. 2(a) the experimental $\sigma_1(\omega, B = 0)$ (solid blue line) can be seen to be in accord with the Drude lineshape (dashed line), as previously reported for pure La$_{0.7}$Sr$_{0.3}$MnO$_3$.[17–20] Good agreement is found above 0.5 THz, while the poorer fit in the 0.3-0.5 THz range is
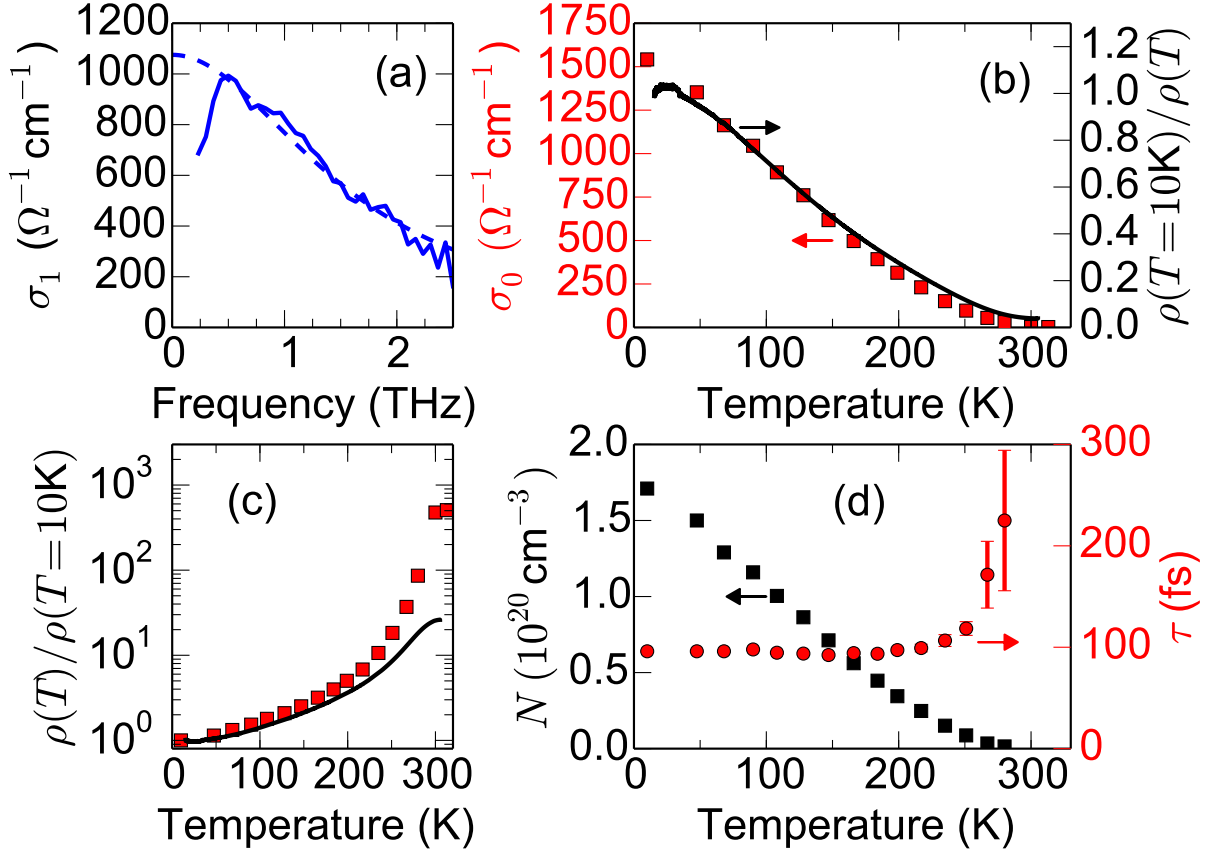
6

discussed below with reference to Fig. 4(d).

Figure 2: (a) Frequency-dependence of σ_1 for the VAN film at $B = 0$ and $T = 86\,\mathrm{K}$ from experiment (solid line) and the Drude-Lorentz model (dashed line). (b) Temperature-dependence of σ_0 for the VAN film (squares, left axis) compared with the normalised dc conductivity $\rho(T = 10\,\mathrm{K})/\rho(T)$ (line, right axis). (c) THz resistivity normalized by resistivity at $10\,\mathrm{K}$ (squares, $\sigma_0(10\,\mathrm{K})/\sigma_0(T)$) compared with the ratio $\rho(T)/\rho(T = 10\,\mathrm{K})$ for dc transport (line). (d) Mobile carrier density N (squares, left axis) and scattering time τ (circles, right axis) for the VAN film, as a function of temperature.

The metal-insulator transition (MIT) of the VAN film was studied at zero magnetic field by examining σ_0 from fits to $\sigma_1(\omega)$ at different temperatures. The squares in Fig. 2(b) indicate σ_0 for the VAN film, which was substantially more conductive at low temperatures, when spins were co-aligned.[23] For comparison, the dc conductivity ratio $\sigma(T)/\sigma(T = 10\,\mathrm{K})$ calculated from $\rho(T = 10\,\mathrm{K})/\rho(T)$ is shown by the solid black line. While the temperature dependence appears similar at low temperatures, at higher temperatures the THz conduc-

tivity drops more rapidly than the dc conductivity. This difference is apparent in Fig. 2(c), where the THz resistivity ratio changes by nearly three orders of magnitude between 10 K and 300 K, while the dc ratio changes by only a factor of 30. The contrasting temperature dependences of the conductivity may be linked to: (i) dissimilar scattering times probed by THz radiation and transport: the transport lifetime is weighted by an additional geometric factor;[24] (ii) different transport masses and optical masses, resulting from the electron-electron interaction, as seen in other polar oxides;[11] (iii) dc and ac conduction arising from distinct physical processes, or probing different length scales.

Drude-Lorentz fits to the experimental $\sigma_1(\omega)$ (assuming a constant $m^* = 3.0 m_e$) yielded the evolution of the carrier density N and scattering time τ with temperature, as indicated in Fig. 2(d). The mobile carrier density peaks at low temperature at $1.7 \times 10^{20} \, \mathrm{cm}^{-3}$, and drops towards T_C. The effective number of carriers per LSMO unit cell is $n_{\mathrm{eff}} \simeq 0.02$ at low temperature, assuming the LSMO is 50 % of the VAN film, and using the unit cell size determined from the X-ray diffraction results in Fig. 1. A similar value of $n_{\mathrm{eff}}(10\,\mathrm{K}) \simeq 0.03$ was previously reported[18] for bulk LSMO crystals with $x = 0.3$.

The carrier momentum scattering time τ reported in Fig. 2(d) is relatively independent of temperature, and increases towards T_C, indicating a reduction in the carrier scattering rate at the lowest densities. Values of the mean-free-path λ can be estimated from $\lambda = v_F \tau$ for Fermi velocity $v_F = \hbar (3\pi^2 N)^{1/3}/m^*$, yielding $\lambda \simeq 7\,\mathrm{nm}$ at 10 K. The mean-free path lowers with increasing temperature due to the rapid reduction in N: by 300 K, $N < 5 \times 10^{17} \, \mathrm{cm}^{-3}$, giving $\lambda < 1\,\mathrm{nm}$. Consequently, carriers remain within the LSMO grains (about 10 nm across[9]) rather than tunneling between grains, and the THz conductivity remains Drude-like across the whole temperature range. This is in contrast to semiconductor nanocomposites with mean-free-paths larger than the grain size, where resonant THz conductivities are observed.[22,25]

The scattering time of the VAN was marginally higher than that of the pure film, perhaps as a consequence of the higher crystalline quality of the VAN evident in Figs. 1(b), (d) and

8

(e). For instance, at 300 K the pure LSMO film had $\tau = 102\,\mathrm{fs}$ while for the VAN $\tau = 112\,\mathrm{fs}$. The mean-free path for the pure film at 300 K was $\lambda \simeq 3\,\mathrm{nm}$, greater than for the VAN, as the carrier density $N = 2.2 \times 10^{19}\,\mathrm{cm}^{-3}$ was higher at this temperature owing to the pure film's larger T_C.

The magnetic field dependence of $\sigma_1(\omega)$ is reported in Fig. 3, cooled without magnetic field from above room temperature. At 50 K [panel (a)] σ_1 can be seen to be large, Drude-like (dashed lines), and to increase slightly for $B = 4\,\mathrm{T}$ (red line) in comparison to $B = 0\,\mathrm{T}$ (blue line). At 200 K [panel (b)] the THz conductivity is Drude-like, and the application of a magnetic field boosts $\sigma_1(\omega)$ more significantly, in a manner consistent with an increase in density from $N(B=0) = 3.5 \times 10^{19}\,\mathrm{cm}^{-3}$ to $N(B = 8\,\mathrm{T}) = 8.0 \times 10^{19}\,\mathrm{cm}^{-3}$ (assuming $m^* = 3m_e$, independent of B). The scattering time reduces at higher field, from $\tau(B = 0) = 94\,\mathrm{fs}$ to $\tau(B = 8\,\mathrm{T}) = 61\,\mathrm{fs}$.

The greater enhancement in $\sigma_1(\omega)$ with B at 200 K in comparison to that at 50 K can be understood within the double-exchange picture of MR in the manganites as follows. The core spins are partially disordered at 200 K [Fig. 1(c)] with a finite angle θ between nearest neighbour spins. Increasing B enhances the alignment of nearest neighbour spins, reducing θ. Both the charge carrier transfer integral for hopping and the magnetization scale with $\cos\theta/2$, and hence both are enhanced by an applied B.[23] At 50 K nearest neighbour core spins exhibit less thermal disorder, and therefore σ_1 does not alter as substantially with B.

$\sigma_1(\omega, B)$ at the MI transition is reported in Fig. 3(c). Although σ_1 is negligible for $B = 0$ (blue line), the application of a magnetic field creates a conductive medium where σ_1 increases with frequency (e.g. purple line, $B = 8\,\mathrm{T}$). This is in stark contrast to the near-Drude behaviour of $\sigma_1(\omega, B)$ below T_C seen in Fig. 3(a) and (b). The enhanced σ_1 with frequency at T_C is matched by a positive σ_2 (not shown) that also increases with frequency. Linear or slightly sub-linear increases in σ_1 and σ_2 with frequency have been widely studied in amorphous semiconductors, with different physical mechanisms yielding the same frequency dependence.[26] The quantum mechanical tunneling of quasiparticles through
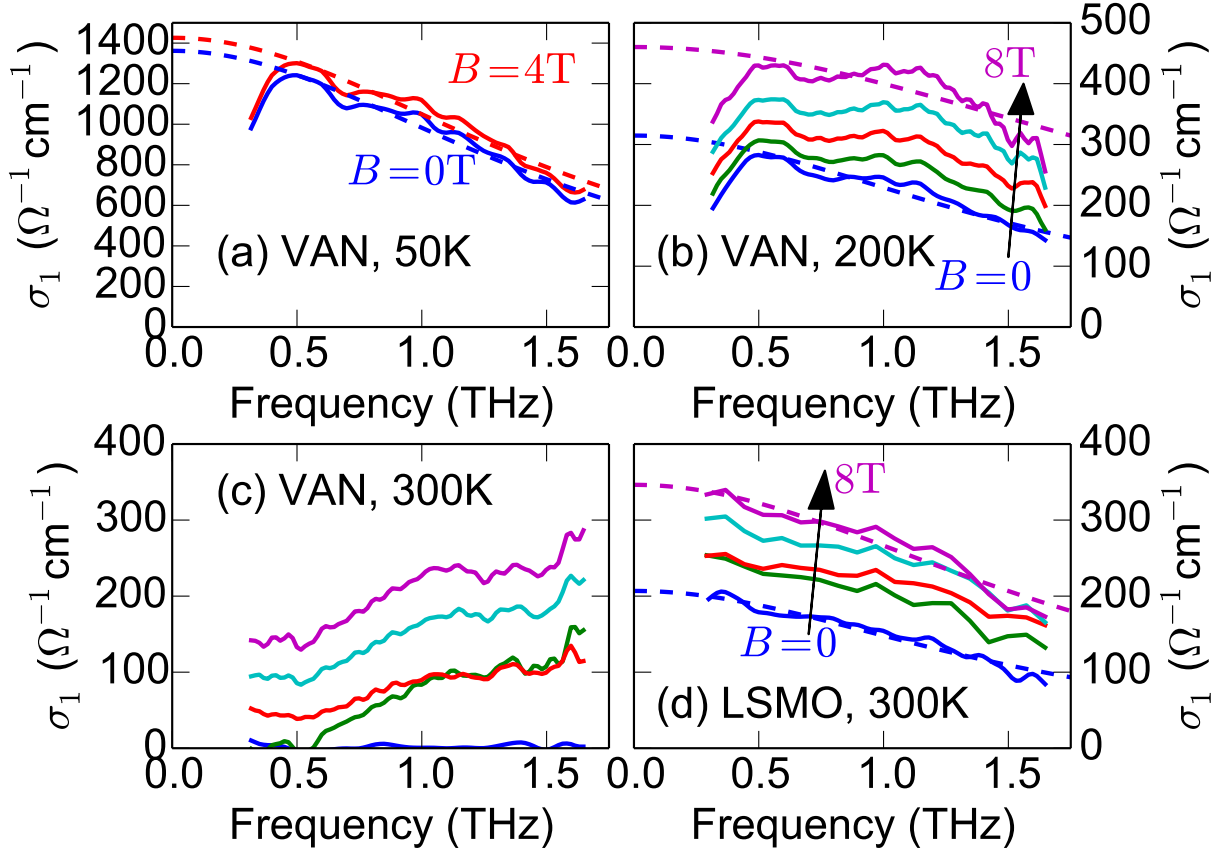
9

Figure 3: (a) The real part of the THz conductivity, σ_1, for the VAN film at $50\,\mathrm{K}$ (solid lines) follows the Drude-Lorentz form (dashed lines) above $0.5\,\mathrm{THz}$, indicative of delocalized electron transport, both at $B = 0\,\mathrm{T}$ (blue) and at $B = 4\,\mathrm{T}$ (red). (b) Similar to (a), but at $200\,\mathrm{K}$, and for $B = 0 \rightarrow 8\,\mathrm{T}$ in $2\,\mathrm{T}$ steps. (c) At $300\,\mathrm{K}$, close to $T_\mathrm{C} = 303\,\mathrm{K}$, the VAN film has negligible σ_1 for $B = 0\,\mathrm{T}$ (blue line), but substantial THz conductivity for $B \geq 2\,\mathrm{T}$ (coloured lines, from $2\,\mathrm{T}$ to $8\,\mathrm{T}$ in $2\,\mathrm{T}$ steps). At low frequencies σ_1 is suppressed. (d) Room-temperature THz σ_1 for the pure LSMO film (lines), and Drude-Lorentz fits (dashed lines).

an energy barrier separating two locations exhibits $\sigma_1 \propto \omega$, for both bare quasiparticles and for small polarons.[26] The thermal excitation of classical carriers over a potential barrier also has the same frequency dependence.[26] Semiconductor nanomaterials have been also reported to show $\sigma_1 \propto \omega$ and a negative σ_2, in the regime where carrier backscattering from interfaces may occur.[22,25]

In the present case the short mean-free path in comparison to the grain size (discussed above), along with the positive σ_2, suggests that the dominant conductive response at THz frequencies is from carriers that oscillate within each LSMO grain, ruling out inter-grain transport. The THz conductivity is therefore a probe of the intrinsic conductivity of each nanocolumn, rather than the extrinsic conductivity associated with spin-polarized tunneling between grains. Intragrain conduction within the VAN has a comparable scattering time (and therefore mobility) to that of pure LSMO, as τ in both cases is similar (see above).

The remarkable increase in $\sigma_1(\omega)$ with applied magnetic field demonstrates that colossal magnetoresistance persists up to THz frequencies. To enable a quantitative comparison between the magnitude of the colossal THz MR, reported here for the first time, with the well-known dc CMR effect, we calculated the magnetoresistance $\Delta\rho/\rho_0 = \sigma_1(B=0)/\sigma_1(B) - 1$, expressed as a percentage. In Fig. 4(a) $\Delta\rho/\rho_0$ is shown as a function of frequency. For the VAN at 50 K, well below $T_C = 303$ K, the THz CMR is small, with $|\Delta\rho/\rho| \leq 8\%$ (green crosses). In contrast, at 200 K the THz CMR is greater and increases with frequency (blue squares). The increase in $\Delta\rho/\rho_0$ with frequency can be understood to result from the shorter τ and larger N under an applied magnetic field: a smaller τ makes $\sigma_1(\omega)$ flatter, enhancing $\Delta\rho/\rho_0$ at high frequencies. The solid lines in Fig. 4(a) show the modelled $\Delta\rho/\rho_0$ from the Drude-Lorentz fits. Note that the Drude picture fails at lower frequencies, where the experimental $\sigma_1(\omega)$ deviates from this simple model [Fig. 2(a)].

While the dc MR vanishes at the Curie temperature,[9] the THz MR is dramatically enhanced by proximity to T_C. At 300 K the THz MR for the VAN film [red triangles in Fig. 4(a) and (b)] can be seen to saturate at close to -100 %. The conductivity changes by over 2
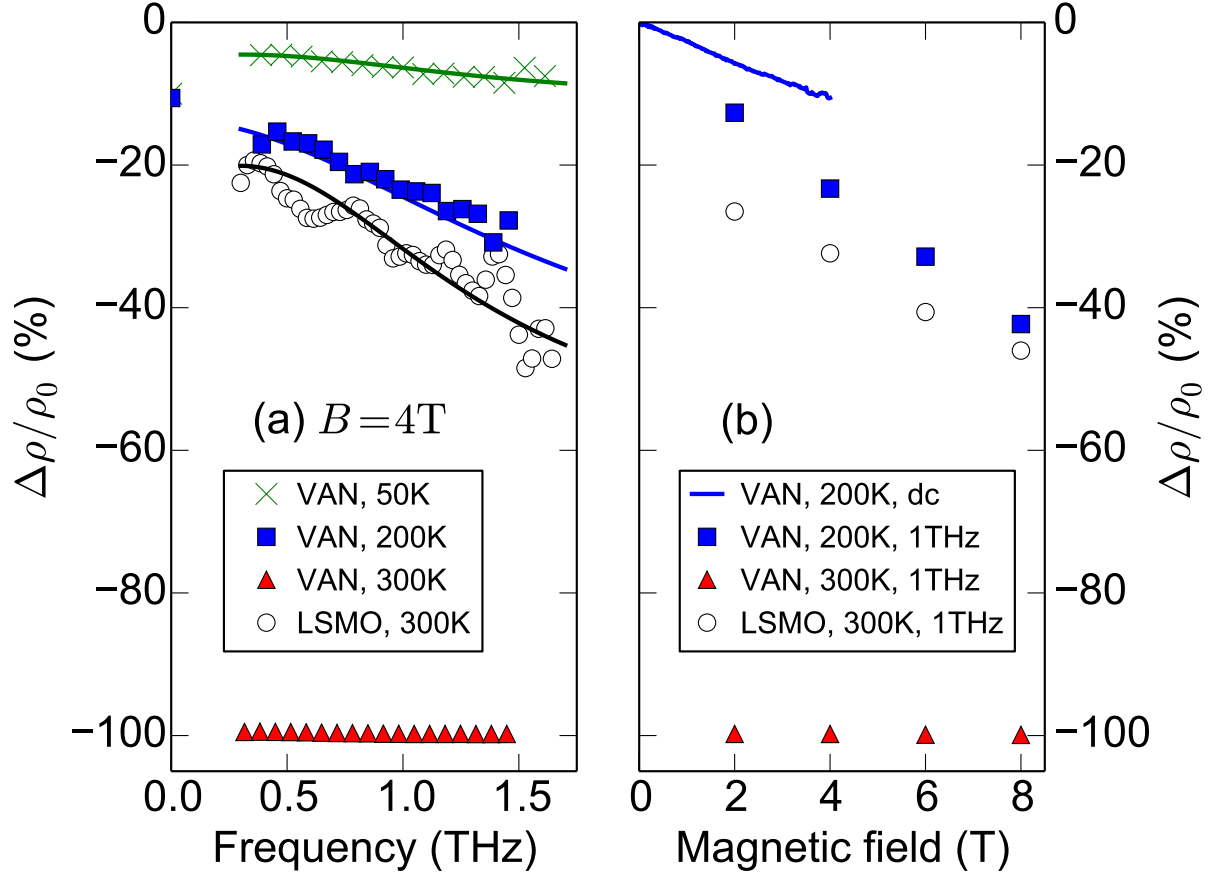
Figure 4: (a) Frequency-dependence of the colossal THz MR of the LSMO-ZnO VAN at $B = 4\,\mathrm{T}$ for $T = 50\,\mathrm{K}$ (green crosses), $T = 200\,\mathrm{K}$ (blue squares) and $T = 300\,\mathrm{K}$ (red triangles). Data for the pure LSMO film at $T = 300\,\mathrm{K}$ are also shown (circles). Fits with the Drude-Lorentz model are given by the solid lines. (b) Magnetic-field dependence of CMR. Data obtained from dc magnetotransport (solid line) on the VAN at $T = 200\,\mathrm{K}$ can be compared with the MR at $1.0\,\mathrm{THz}$ (blue squares). At $300\,\mathrm{K}$ and $1.0\,\mathrm{THz}$, the THz MR approaches $100\,\%$ for the VAN (red triangles), while it is smaller for the pure LSMO film (circles).

orders of magnitude: for instance, at $1.0\,$THz, $\sigma(B = 2\,\text{T})/\sigma(B = 0) = 400$. Thus the THz MR is significantly higher than the largest dc MR reported for LSMO VANs ($\Delta\rho/\rho_0 = -30\,\%$ at $154\,$K and $B = 1\,$T).[9] At room temperature, dc MR is small for the LSMO VANs, at $\Delta\rho/\rho_0 < 5\,\%$.[9] Since the THz conductivity probes local carrier motion within a LSMO grain, this suggests that on nanometre length scales the MR can be large, even when it is small on the macroscopic length scales probed by dc transport.

The increase observed in $\Delta\rho/\rho_0$ close to T_C suggests an intrinsic origin for the THz CMR effect in the VAN film, in contrast to the extrinsic effect (spin-polarized tunneling) that dominates the dc CMR effect. The pure LSMO film may therefore also be expected to have substantial THz CMR. In Fig. 3(d) the THz conductivity $\sigma_1(\omega, B)$ is reported for the pure LSMO film at $T = 300\,$K, below $T_\text{C} = 353\,$K. In this case the frequency-dependent conductivity is Drude-like over the whole frequency range. This enables the reduction in $\sigma_1(\omega)$ in the 0.3-0.5 THz range for the VAN film [evident in Figs. 2 and 3(a), (b)] to be linked to the effective-medium nature of the $La_{0.7}Sr_{0.3}MnO_3$:ZnO film, or to a plasmon response.[22,27] Large increases in σ_1 with B can be observed in Fig. 3(d), similar to the VAN film at $200\,$K. The THz MR for the pure LSMO film is also reported in Fig. 4. Both the frequency and magnetic field dependences of $\Delta\rho/\rho_0$ are similar to the VAN $200\,$K results, where extra mobile (Drude-like) electrons were created under a magnetic field. The magnitude of the THz CMR for the pure film is sizable, e.g. $\Delta\rho/\rho_0 = -27\,\%$ at $B = 2\,$T, $300\,$K and $1.0\,$THz. In comparison, the dc MR for pure LSMO is smaller, peaking at $\Delta\rho/\rho_0 = -6.4\,\%$ at $280\,$K under $B = 1\,$T.[9] The relative change in conductivity $\sigma(B = 2\,\text{T})/\sigma(B = 0) = 1.36$ at $300\,$K and $1.0\,$THz for the planar film is smaller than for the VAN ($\sigma(B = 2\,\text{T})/\sigma(B = 0) = 400$), as the planar material is still conductive at $B = 0$ (at $300\,$K it remains below T_C).

While both the vertically-aligned nanostructures and the pure LSMO film were found to exhibit sizable THz CMR, the VAN concept is more attractive for future THz devices. For instance, the VAN film thickness can be readily scaled to maximise the change in THz transmission, without shifting the Curie temperature. This may enable THz filters where

the attenuation can be tuned by an applied magnetic field. Subsequent in-plane patterning of the VAN film would allow the creation of THz wire-grid polarisers with a transmission that can be tuned by temperature and/or magnetic-field.

In the following we discuss some of the different physical models of the intrinsic CMR effect in the manganites. The charges in these models can be categorised as either (i) free charges unimpeded by the polar lattice ions, or (ii) polarons strongly coupled to the lattice. In Ramakrishnan et $al.$'s approach, a broad band of mobile electrons derived from Mn 3d e_g states (labeled b) coexists with a narrow band of localized polarons (labeled l).[28] The predicted mobile carrier fraction for the b-band is $n_{eff} < 0.1$, in agreement with the results herein ($n_{eff} \simeq 0.02$ at 10 K for the VAN), where the electron density is low in comparison to $1 - x = 0.7$. Alternatively, manganites have been described as magnetic charge-transfer insulators, with transport ascribed to holes with oxygen p-like character coupled to local moments on the Mn^{3+} ions.[29] At low temperatures the ferromagnetic exchange interaction with the Mn d electrons breaks the p-like bipolarons into mobile hole polarons, with a peak n_{eff} at low temperature equal to the hole doping level $x = 0.25$.[29] The small n_{eff} from THz spectroscopy reported here is closer to the e_g b-band description, rather than the p-like hole polaron model, but further work is needed.

The enhanced σ_1 (larger absorption) with frequency reported in Fig. 3(c) under a magnetic field may likewise be described within either the free carrier or the polaron pictures of charge transport. Both bare charges and small polarons have $\sigma_1 \propto \omega$ in amorphous semiconductors,[26] as discussed above. Alternatively, the increase in σ_1 with frequency may result from a change in the spectral weight of a broad infrared absorption feature between 0.5 and 1.0 eV, which changes significantly with B near T_C.[1,18,30] This infrared absorption of bulk LSMO was attributed to interband O 2p$\rightarrow$ Mn 3d e_g transitions,[18] although the exact assignment of features has been debated.[1,30] Alexandrov et $al.$ offered the explanation that the transfer of spectral weight to lower frequencies upon lowering T_C or increasing B was due to the breaking of bipolarons into polarons.[15,16] The polaron and bipolaron contri-

butions to $\sigma_1(\omega)$ were modelled as broad, Gaussian-like resonances with a finite σ_1 in the THz range.[15,16] However, the conductivity model used diverges as $\omega \to 0$, and hence does not adequately reproduce the experimental Drude-like peak in $\sigma_1(\omega)$ at zero ω for $B = 0$, or the observation that $\sigma_1(\omega) \to 0$ as $\omega \to 0$ for $B \geq 2\,\mathrm{T}$. Alternative descriptions of $\sigma_1(\omega)$ for small polarons derived from dynamical mean-field theory may suffice.[31]

Other approaches, including phase separation and percolation models, have also been explored to understand the electrical properties of the manganites,[1,4,32] but the optical conductivity of these models has yet to be studied. While other oxides with long-range magnetic or charge order have resonant absorption features in the THz range, resulting from electro-magnons[33,34] or charge density waves,[35] these are not at present thought to contribute in $La_{0.7}Sr_{0.3}MnO_3$, although nanoscale charge ordered phases have been reported in manganites.[32]

In conclusion, the colossal magnetoresistance exhibited by manganite films been demonstrated to persist to THz frequencies for both vertically-aligned nanostructures of LSMO and for planar LSMO thin films. The THz magnetoresistance was found to exceed the dc magnetoresistance, and to approach -100 % at the Curie temperature in magnetic fields of $2\,\mathrm{T}$ for the VAN. Below the Curie temperature the Drude-like THz conductivity signified band-like transport for both pure LSMO and VAN films with small mean-free paths compared to the grain sizes, indicating that hopping between grains is not important at THz frequencies. At the Curie temperature the application of a magnetic field produced a non-Drude conductivity, with the real part increasing monotonically with frequency, and possible origins of this trend were discussed. The local charge transport within a ferromagnetic grain probed by THz radiation was substantially larger than often found in macroscopic device transport measurements. This suggests the promise of this material system for future THz optical and electronic components, such as magnetically-driven modulators. Future work will study the VAN at higher temperatures, into the insulating phase, and the planar film at and above the Curie temperature. By examining VAN films with different grain sizes and/or fill fractions

the role of interfacial scattering will be explored.

Methods

$La_{0.7}Sr_{0.3}MnO_3$-ZnO VANs and planar $La_{0.7}Sr_{0.3}MnO_3$ thin films were fabricated by pulsed laser deposition. A $\lambda = 248\,nm$ KrF excimer laser (Lambda Physik) was focussed onto the target with a fluence of $4.5\,Jcm^{-2}$ and a repetition rate of $1\,Hz$. During deposition an oxygen pressure of $26.7\,Pa$ was introduced to the chamber and the substrate was heated to $477\,K$. After deposition the samples were cooled to room temperature at a rate of $20\,Kmin^{-1}$ under an oxygen pressure of $26.7\,kPa$ to ensure full oxygenation. Both films were $200\,nm$ thick.

A SQUID magnetometer (Quantum Design MPMS-5S) determined the zero-field-cooled (ZFC) and field-cooled (FC) magnetization of the samples versus temperature, under $B = 10\,mT$. A four-circle x-ray diffractometer (PANalytical Xpert Pro MRD) with a Cu source and a 4-bounce hybrid monochromator was used to give pure K-α_1 radiation (λ=1.540598 Å). A Pixcel detector was used in scanning mode to collect the $2\theta - \omega$ diffraction scans. Reciprocal space maps were obtained from a collection of $2\theta - \omega$ scans in scanning mode.

Terahertz time-domain spectroscopy (THz-TDS) allowed the complex optical conductivity $\sigma(\omega) = \sigma_1(\omega) + i\sigma_2(\omega)$ to be determined over the frequency range applicable for intraband transport.[22] THz-TDS was performed under a magnetic field $B \leq 8\,T$ oriented parallel to the growth axis, as shown in Fig. 1(a), using a custom-made spectrometer with a bandwidth of $1.7\,THz$. The transmission of the films was obtained at normal incidence, thereby probing charge transport within and between grains. The incident THz beam was linearly polarized along the substrate's [110] direction, in order to avoid birefringence effects in $LaAlO_3$.[21] The accessible temperature range in the variable temperature insert of the superconducting magnet was between $2\,K$ and $300\,K$. Measurements from higher temperatures ($400\,K$) down to $80\,K$ were performed on a separate spectrometer at $B = 0$, with samples mounted in a nitrogen cryostat, and with a wider bandwidth of $2.5\,THz$.

Acknowledgements

Note: The authors declare no competing financial interest.

References

(1) Ziese, M. *Rep. Prog. Phys.* **2002**, *65*, 143–249.

(2) Park, J.-H.; Vescovo, E.; Kim, H.-J.; Kwon, C.; Ramesh, R.; Venkatesan, T. *Nature* **1998**, *392*, 794–796.

(3) Kang, B. S.; Wang, H.; MacManus-Driscoll, J. L.; Li, Y.; Jia, Q. X.; Mihut, I.; Betts, J. B. *Appl. Phys. Lett.* **2006**, *88*, 192514.

(4) Siwach, P. K.; Singh, H. K.; Srivastava, O. N. *J. Phys.-Condens. Matter* **2008**, *20*, 273201.

(5) Kang, Y. M.; Kim, H. J.; Yoo, S. I. *Appl. Phys. Lett.* **2009**, *95*, 052510.

(6) MacManus-Driscoll, J. L. *Adv. Funct. Mater.* **2010**, *20*, 2035–2045.

(7) Bi, Z. X.; Weal, E.; Luo, H. M.; Chen, A. P.; MacManus-Driscoll, J. L.; Jia, Q. X.; Wang, H. Y. *J. Appl. Phys.* **2011**, *109*, 054302.

(8) MacManus-Driscoll, J.; Suwardi, A.; Wang, H. *MRS Bulletin* **2015**, *40*, 933–942.

(9) Chen, A.; Bi, Z.; Tsai, C.-F.; Lee, J.; Su, Q.; Zhang, X.; Jia, Q.; MacManus-Driscoll, J. L.; Wang, H. *Adv. Funct. Mater.* **2011**, *21*, 2423.

(10) Lloyd-Hughes, J. *J. Phys. D-Appl. Phys.* **2014**, *47*, 374006.

(11) Lloyd-Hughes, J.; Failla, M.; Ye, J.; Jones, S. P. P.; Teo, K. L.; Jagadish, C. *Appl. Phys. Lett.* **2015**, *106*, 202103.

(12) Failla, M.; Myronov, M.; Morrison, C.; Leadley, D. R.; Lloyd-Hughes, J. *Phys. Rev. B* **2015**, *92*, 045303.

(13) Ikebe, Y.; Morimoto, T.; Masutomi, R.; Okamoto, T.; Aoki, H.; Shimano, R. *Phys. Rev. Lett.* **2010**, *104*, 256802.

(14) Jin, Z.; Tkach, A.; Casper, F.; Spetter, V.; Grimm, H.; Thomas, A.; Kampfrath, T.; Bonn, M.; Kläui, M.; Turchinovich, D. *Nat. Phys.* **2015**, *11*, 761–766.

(15) Alexandrov, A. S.; Bratkovsky, A. M. *Phys. Rev.B* **1999**, *60*, 4.

(16) Alexandrov, A. S.; Bratkovsky, A. M. *J. Phys.-Condens. Matter* **1999**, *11*, L531–L539.

(17) Okimoto, Y.; Katsufuji, T.; Ishikawa, T.; Urushibara, A.; Arima, T.; Tokura, Y. *Phys. Rev. Lett.* **1995**, *75*, 109–112.

(18) Okimoto, Y.; Katsufuji, T.; Ishikawa, T.; Arima, T.; Tokura, Y. *Phys. Rev. B* **1997**, *55*, 4206–4214.

(19) Averitt, R. D.; Lobad, A. I.; Kwon, C.; Trugman, S. A.; Thorsmølle, V. K; Taylor, A. J. *Phys. Rev. Lett.* **2001**, *87*, 017401.

(20) Averitt, R. D.; Taylor, A. J. *J. Phys.-Condens. Matter* **2002**, *14*, R1357.

(21) Lloyd-Hughes, J.; Jones, S. P. P.; Castro-Camus, E.; Doig, K. I.; MacManus-Driscoll, J. L. *Opt. Lett.* **2014**, *39*, 1121–1124.

(22) Lloyd-Hughes, J.; Jeon, T.-I. *J Infrared Milli Terahz Waves* **2012**, *33*, 871.

(23) Hundley, M. F.; Hawley, M.; Heffner, R. H.; Jia, Q. X.; Neumeier, J. J.; Tesmer, J.; Thompson, J. D.; Wu, X. D. *App. Phys. Lett.* **1995**, *67*, 860.

(24) Kabir, N. A.; Yoon, Y.; Knab, J. R.; Chen, J. Y.; Markelz, A. G.; Reno, J. L.; Sado-fyev, Y.; Johnson, S.; Zhang, Y. H.; Bird, J. P. *Appl. Phys. Lett.* **2006**, *89*, 132109.

(25) Ulbricht, R.; Hendry, E.; Shan, J.; Heinz, T. F.; Bonn, M. *Rev. Mod. Phys.* **2011**, *83*, 543–586.

(26) Elliott, S. *Advances in Physics* **1987**, *36*, 135–217.

(27) Parkinson, P.; Lloyd-Hughes, J.; Gao, Q.; Tan, H. H.; Jagadish, C.; Johnston, M. B.; Herz, L. M. *Nano Lett.* **2007**, *7*, 2162–2165.

(28) Ramakrishnan, T. V.; Krishnamurthy, H. R.; Hassan, S. R.; Pai, G. V. *Phys. Rev. Lett.* **2004**, *92*, 157203.

(29) Alexandrov, A. S.; Bratkovsky, A. M. *Phys. Rev. Lett.* **1999**, *82*, 141–144.

(30) Quijada, M.; Černe, J.; Simpson, J. R.; Drew, H. D.; Ahn, K. H.; Millis, A. J.; Shree-kala, R.; Ramesh, R.; Rajeswari, M.; Venkatesan, T. *Phys. Rev. B* **1998**, *58*, 16093–16102.

(31) Fratini, S.; Ciuchi, S. *Phys. Rev. B* **2006**, *74*, 075101.

(32) Tao, J.; Niebieskikwiat, D.; Varela, M.; Luo, W.; Schofield, M. A.; Zhu, Y.; Sala-mon, M. B.; Zuo, J. M.; Pantelides, S. T.; Pennycook, S. J. *Physical Review Letters* **2009**, *103*, 097202.

(33) Pimenov, A.; Mukhin, A. A.; Ivanov, V. Y.; Travkin, V. D.; Balbashov, A. M.; Loidl, A. *Nat. Phys.* **2006**, *2*, 97–100.

(34) Jones, S. P. P.; Gaw, S. M.; Doig, K. I.; Prabhakaran, D.; Hétroy Wheeler, E.; Boothroyd, A. T.; Lloyd-Hughes, J. *Nat. Commun.* **2014**, *5*, 3787.

(35) Lloyd-Hughes, J.; Prabhakaran, D.; Boothroyd, A. T.; Johnston, M. B. *Phys. Rev. B* **2008**, *77*, 195114.

Graphical TOC Entry